Polymer Bulletin (2019) 76:4967–4989
https://doi.org/10.1007/s00289-018-2643-0

ORIGINAL PAPER

Chemically modified vermiculite clay: a means to remove emerging contaminant from polluted water system in developing nation

Adewale Adewuyi[1] · **Rotimi Ayodele Oderinde**[2]

Received: 27 October 2018 / Revised: 27 November 2018 / Accepted: 28 November 2018 /
Published online: 4 December 2018
© Springer-Verlag GmbH Germany, part of Springer Nature 2018

Abstract

The performance of chemically modified vermiculite clay (VCM) and unmodified vermiculite clay (VCL) was evaluated for the removal of 4-aminoantipyrine from aqueous solution. The chemical modification of VCL was achieved using cellulose nanocrystals and nitrilotriacetic acid via facile dispersion and intercalation. After the modification, the BET surface area of VCL increased from 4 to 96 $m^2\ g^{-1}$ in VCM. The removal of 4-aminoantipyrine was pH dependent which followed pseudo-second-order kinetics. Langmuir isotherm model provided the best fit for the sorption data while a percentage removal of 4-aminoantipyrine unto VCM of up to 98.410% was attained. Quantum chemical computational analysis was also used to describe the sorption process in molecular terms. The lowest unoccupied molecular orbital and highest occupied molecular orbital are distributed over the molecule of 4-aminoantipyrine, and interaction between the surfaces of VCL/VCM and 4-aminoantipyrine may have occurred via donor–acceptor interactions. A regeneration capacity of 76% was obtained for VCM while that of VCL was 60%. The study has revealed that the property of vermiculite clay can be improved via facile dispersion and intercalation with the potential of removing pharmaceutical pollutants from water system.

Keywords 4-Aminoantipyrine · Adsorption · Pharmaceutical waste · Vermiculite · Wastewater

✉ Adewale Adewuyi
walexy62@yahoo.com

[1] Department of Chemical Sciences, College of Natural Sciences, Redeemer's University, Ede, Osun State, Nigeria

[2] Industrial Unit, Department of Chemistry, University of Ibadan, Ibadan, Oyo State, Nigeria

Introduction

The presence of organic compounds in the environment is of increasing concern due to their eco-toxicological effects. Some of these organic compounds are pharmaceutical agents with therapeutic importance, but when they get into the environment, especially water bodies, they become pollutant either directly or indirectly depending on their metabolites. Excessive use of pharmaceutical agents can create serious problems to the environment. The human or animal body may not be able to completely breakdown some of the dose when taken, and as a result such dose will have to be excreted as active compound [1]. On the other hand, a few of these pharmaceutical agents can also serve as reagents for biochemical reactions. When used as reagent, removal of these pharmaceutical agents after reaction is a concern. They are sometimes in industrial effluents from pharmaceutical industries, and there are cases where they are in laboratory wastes when used as reagents during chemical or biochemical reactions. This is a major problem in developing countries like Brazil and Nigeria. Presently in Brazil and Nigeria, there is need to develop an effective means of treating effluents from hospitals, pharmaceutical industries and laboratories (most especially academic institution based laboratories).

4-Aminoantipyrine is an example of pharmaceutical agent that serves as drug as well as biochemical reagent. Apart from being able to act as an analgesic and anti-inflammatory agent, 4-aminoantipyrine is used in the assay for aspartate aminotransferase or glutamate oxalacetate transaminase. Although it poses the risk of agranulocytosis, 4-aminoantipyrine can measure extracellular water. Studies have shown its use as a redox indicator during the determination of free and captured glucose oxidase [2, 3]. Studies have revealed the significance of its derivatives as biological and pharmacological agents [4, 5]. Currently, 4-aminoantipyrine is receiving large attention because of the important role it plays as potential pharmaceutical and biochemical reagent. Due to its continuous and excessive use, its presence has been detected in water at low concentration, which has created a serious concern. Developing an effective process for purifying water contaminated with low concentration of 4-aminoantipyrine is a challenge in developing nations, and this is the core focus of this present study.

Use of adsorption as a water purification process is economical and capable of removing organic pollutants from water system. Adsorption has played important role in the removal of low concentrations of organic pollutants from wastewater, aqueous solution, potable water and process effluents [6]. Although several materials such as activated carbon, zeolite and biomass are used as adsorbent to achieve this, but some of them have shortcomings such as inefficient removal, high cost, inefficient desorption and regeneration. There is need to develop new adsorbent that will circumvent these shortcomings. There may also be need for search for cheap, readily available and environmentally friendly materials that may be directly used or serve as base material for this purpose. Use of clay materials may meet this need as they can serve as viable adsorbent for the adsorption of organic compounds.

Vermiculite is a type of clay that may be suitable for this use [7]. It is a hydrous phyllosilicate mineral and trioctahedral with negative charges resulting from the

substitution of Si^{4+} by trivalent cations in tetrahedral positions [8–10]. Depending on the water interlamellar layers and interlayer cations, vermiculites have a structural unit thickness of about 1.4 nm with the water interlamellar layers susceptible to hydration and dehydration processes [11]. The interlayer cations—Mg^{2+} and minor amounts of Ca^{2+}, Na^{+}, and K^{+} play a key role in the hydration properties, influenced by cation radius and charge. The cation exchange capacity (CEC) varies between the 120 and 200 $cmol^{+}/kg$ for air-dried vermiculites or 140 and 240 $cmol^{+}/kg$ for dehydrated vermiculites [10, 12]. Figure 1 presents the structural model of vermiculite from Brazil [10]. Vermiculite is abundantly present in Brazil, and there is need to find application for this naturally abundant resource in this part of the world. Use of vermiculite as a means of purifying 4-aminoantipyrine contaminated water will be an excellent way of finding application for this abundant resource in Brazil and other developing countries like Nigeria.

Vermiculite expands significantly when heated which indicates that the properties of vermiculite may improve via intercalation or through other chemical reactions. Previous works have shown that it can be expanded to produce highly porous materials for technological and environmental applications [13–17]. Modifying the surface properties of vermiculite is a key way to improve its capacity for specific applications such as in water purification. As an adsorbent, it may be modified by various means with the objective of increasing the adsorption capacity. This is achievable by enhancing the bond strength between the adsorbate and vermiculite (the adsorbent). Previous studies have shown that facile dispersion of cellulose nanocrystals (CNCs) on the surface and internal layers of expanded vermiculite can improve its properties and capacity for specific applications [17, 18]. Based on the ability of vermiculite to expand, the present study aims at improving the wastewater purifying capacity of vermiculite by modification via facile dispersion and intercalation of the expanded vermiculite with CNCs followed by surface functionalization with NTA.

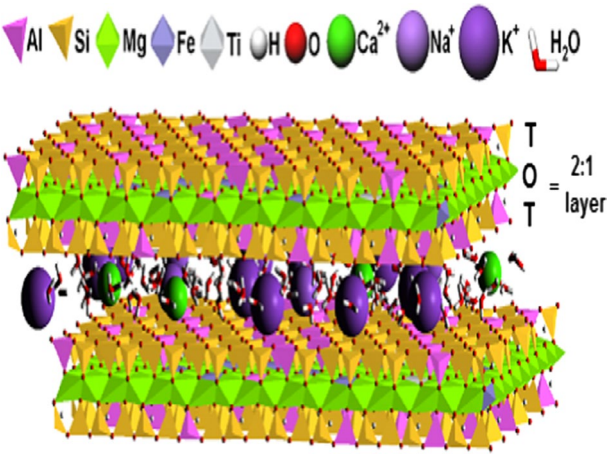

Fig. 1 Model of the structure of vermiculite from Brazil (Valášková and Martynková [10])

Experimental

Materials

As previously reported [16], vermiculite was supplied by Vermiculita Ind. Com. (Brazil) with granulometry 0.3–0.6 cm and approximate composition $(Al_{0.30}Ti_{0.04}Fe_{0.63}Mg_{2.00})$ $(Si_{3.21}Al_{0.79})(O_{10}(OH)_2Mg_{0.13}Na_{0.02}K_{0.10}(H_2O)_n)$. NTA and all other chemicals used in this study were purchased from Sigma-Aldrich (Belo Horizonte, Brazil) while 4-aminoantipyrine was purchased from Sigma-Adrich (Germany). Cellulose was obtained from eucalyptus kraft wood pulp with high alpha-cellulose content (96–98%).

Preparation of CNCs

The CNCs were prepared from cellulose via sulfuric acid hydrolysis as described by de Mesquita et al. [19]. Briefly, cellulose was added to 64 wt% sulfuric acid under vigorous mechanical stirring using a Fisatom mechanical stirrer for 25 min. After hydrolysis, the dispersion was diluted tenfold, and the suspensions washed using two-repeated centrifuge cycling at 7000 rpm for 10 min. This was dialyzed with deionized water to remove any non-reactive sulfate groups, salts and sugar until the solution reached pH 7.0. The purified suspension was ultrasonicated using a Cole Parmer ultrasonic processor (model CV 334, 20 kHz) for 30 min. Powdery CNCs were finally obtained by freeze-drying.

Preparation of VCM

VCL (38 g) of 3 m mesh size was dipped in CNCs (0.88%) for 1 h. After the dipping, the VCL–CNCs obtained were dried at 65 °C for 3 h in an oven. This step of dipping VCL in CNCs was repeated four times (4-cycles). NTA was imprinted on VCL–CNCs by simple reaction. To achieve this, 10 g of NTA was placed in a two-necked round bottom flask containing 100 mL deionized water. The temperature was kept at 60 °C and stirred for 1 h. VCL–CNCs was accurately weighed and poured into the flask, while the temperature was gently raised to 70 °C. Sodium methoxide was added, while refluxing for 18 h. The final product was filtered, washed severally with deionized water and oven-dried at 50 °C to obtain the VCM.

Characterization

VCL and VCM were blended with KBr, pressed into pellets and analyzed for their functional groups composition using FTIR (FTIR, Perkin Elmer, spectrum RXI 83303, MA, USA) in the range of 400–4500 cm^{-1}. Thermogravimetric analysis of VCL and VCM was carried out using DTA-TG equipment (C30574600245, Shimadzu, Tokyo, Japan). The X-ray diffraction pattern of VCL and VCM was recorded from 10° to 80° (2θ) with a scanning speed of 2.00°/min using X-ray diffractometer (XRD-7000X-Ray diffractometer, Shimadzu) with filtered Cu Kα radiation operated

at 40 kV and 40 mA. The surface area was determined by nitrogen adsorption using the BET method in a Quantachrome Autosorb IQ_2 instrument while surface morphology was obtained using SEM–EDS (FEI quanta 200 3D, dual beam FEG, model EDAX EDS brand, Bruker) with powdered samples being coated with gold using the sputtering technique in order to increase electrical conductivity and the quality of the micrographs. Particle size distribution and zeta potential were recorded using a zeta potential analyzer (DT1200, Dispersion technology) at 25 °C while observing general calculation model for irregular particles. Measurements of the zeta potential and particle size distribution were read using Dispersion technology-AcoustoPhor Zeta size 1201 software (version 5.6.16).

Adsorption experiment

Batch adsorption experiments were performed at room temperature (298 K) on a rotary shaker using 0.1 g of adsorbent (VCL or VCM) in 250 mL Erlenmeyer's flasks at different initial concentrations of 4-aminoantipyrine (100 mL) ranging from 1 to 5 mg L^{-1}. All the experiments were performed at a shaking speed of 200 rpm for 3 h. The experimental equilibrium time of 3 h was established after several experimental trials at 298 K and 200 rpm. The concentration of 4-aminoantipyrine was monitored by spectrophotometric analysis using a Schimadzu UV–Vis spectrophotometer (model: UV-1650 PC, Schimadzu corporation, Kyoto, Japan) at a wavelength of 244 nm. The amount of 4-aminoantipyrine adsorbed by VCL and VCM was calculated using equation:

$$q_e = \frac{(C_o - C_e)V}{M} \tag{1}$$

where q_e is the amount adsorbed in mg g^{-1}, C_o and C_e are initial and final concentrations (mg L^{-1}) of 4-aminoantipyrine in solution, respectively; V and M are volumes (L) of 4-aminoantipyrine solution and weight (g) of adsorbent (VCL and VCM) used.

Desorption studies

The desorption study was carried out in the presence of ethanol, distilled water, benzene, 0.5 M HCl, 0.5 M NaOH and acetone. VCL and VCM were loaded with 4-aminoantipyrine by contacting 0.1 g of VCL or VCM with 4-aminoantipyrine (1 mg L^{-1}) in 250 mL Erlenmeyer's flasks at room temperature. This was performed at a shaking speed of 200 rpm for 2 h. The 4-aminoantipyrine loaded VCL and VCM were dried at room temperature for 72 h. In order to determine the desorption capacity, 4-aminoantipyrine loaded VCL and VCM were separately poured into different 250-mL Erlenmeyer's flasks containing 100 mL ethanol, distilled water, benzene, 0.5 M HCl, 0.5 M NaOH and acetone. These were shaken at room temperature and at a speed of 200 rpm for 2 h. The desorbed 4-aminoantipyrine was measured by spectrophotometric analysis using a Schimadzu UV–Vis spectrophotometer (model:

UV-1650 PC, Schimadzu corporation, Kyoto, Japan) at a wavelength of 244 nm. Desorption of 4-aminoantipyrine from VCL and VCM was calculated as:

$$\text{Desorption}\,(\%) = \frac{q_e\,(\text{desorption})}{q_e\,(\text{adsorption})} \times 100 \tag{2}$$

Quantum chemical parameters

All theoretical calculations were performed using the DFT electronic structure programs at B3LYP/6-31G level theory using Spartan 14.1 software. The molecular electronic structure of 4-aminoantipyrine was modeled, including the distribution of frontier molecular orbitals in order to establish the reactivity of 4-aminoantipyrine as well as its active sites for the adsorption process.

Results and discussion

Preparation of VCM and characterization

The preparation of VCM is described as shown in Fig. 2. Vermiculite is a phyllosilicate mineral, which is hydrous in nature. When heated, it expands quickly to produce a lightweight material. If the heating is rapid, vermiculite exfoliates as the interlayer water turns into steam, forcing the silicate layers apart from one another in an accordion like expansion (VCL in Fig. 2) with expansion ratio of 20–30 times its original thickness depend on the temperature and time of processing [20, 21].

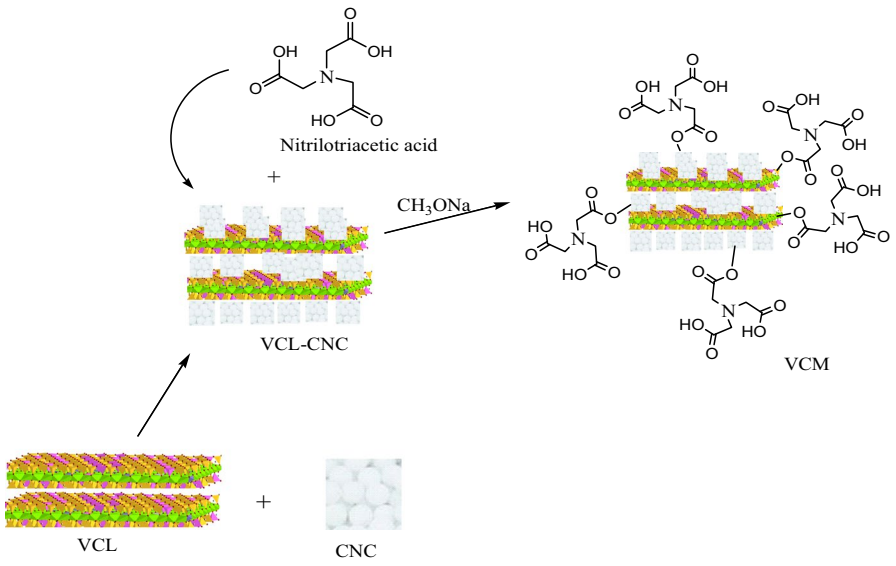

Fig. 2 Schematic representation of the production of VCM

This expansion of vermiculite on heating allows the dispersion of the CNCs into the space created from the expansion. CNCs were deposited on the surface of VCL. This facile dispersion and intercalation of VCL may be due to the capacity of CNCs to facially diffuse throughout VCL and the possibility of hydrogen bonding taking place between VCL and CNCs. The functionalization may be explained as being esterification reaction and facial diffusion. The reaction was catalyzed by the sodium methoxide. Since both VCL and CNCs contains hydroxyl (OH) functional group, the functionalization took place between the OH group and the carboxylic group of the NTA.

Figure 3 reveals the functional groups present in VCL, CNCs and VCM. Bands were observed at 3564 and 3419 cm^{-1} in both VCL and VCM, which were attributed to the –OH functional group of the interlayer water molecules and the silanol groups. Presence of –OH functional group was also found in CNCs at 3406 cm^{-1}. The band for the –OH functional group is broader in VCM than VCL which may be due to the contribution of –OH group from CNCs and NTA. All the samples exhibited a peak at 1640 cm^{-1} that was considered as being due to the –OH bending vibrational frequency of internally bonded water molecules present in the samples. Both VCL and VCM showed strong bands at 1012 cm^{-1}, which were related to the Si–O stretching vibration. They both also exhibited weak bands at 756 and 667 cm^{-1} which were attributed to bending vibrations of Al–OH and Al–O, respectively [22]. The Si–O–Mg bending vibration was also seen in VCL and VCM at 451 cm^{-1} [23]. The band at 1058 cm^{-1} in CNCs and VCM was assigned to C–O–C pyranose ring stretching vibration, and this band is absent in VCL which suggests the presence of CNCs in VCM. The vibrational frequencies found at 1163 cm^{-1} and 1112 cm^{-1} in CNCs were considered as being due to the C–C ring breathing band and C–O–C glycosidic ether band from the polysaccharide component, respectively. These bands were found in VCM but not in VCL; the presence of these bands further suggests the presence of molecules of CNCs in VCM. Bands at 2921 cm^{-1} in VCM and CNCs were attributed to C–H stretching of CH_2 group while bands at 1315 cm^{-1} was assigned to the bending vibration of C–O bonds in the polysaccharide rings [24]. The bands at 1411 and 1327 cm^{-1} found only in VCM were due to the carboxylic

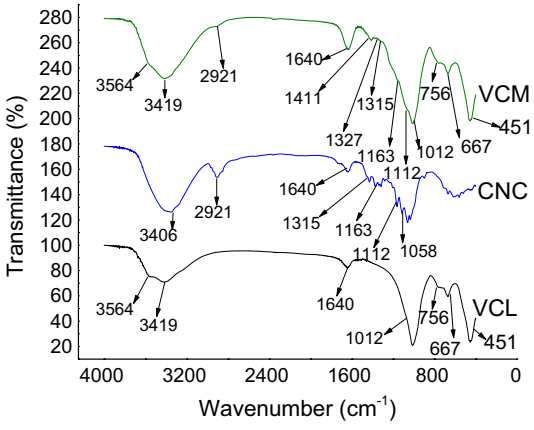

Fig. 3 FTIR of VCL, CNC and VCM

acid deprotonated strong symmetric stretching of COO^- group emanating from the surface functionalization of VCM with NTA.

Figure 4 shows the XRD analysis of VCL, CNCs and VCM, which presented broad and weak reflections. The result indicated that VCL and VCM contains mainly vermiculite, small amounts of mica, illite and hydrobiotite. The pattern shows multiple reflections, suggesting mixture of different minerals as previously reported [25, 26]. The basal spacing (d_{001}) of VCM is larger than that of VCL which suggested the dispersion of CNCs in the layers of VCL to form VCM. The diffractogram further revealed a prominent reflection at 22.60° (**X**) in CNCs which appeared at 24.20° (**X**) in VCM indicating the intercalation of the starting material with CNCs. The modification with CNCs and NTA decreased the intensity of basal reflections of VCL. This observation may be due to the partial transformation of the ordered structure of vermiculite clay into delaminated structure [27]. This may have facilitated the intercalation of bigger chemical species like CNCs. Smaller chemical species like NTA are capable of acting as chelating agents toward exchangeable cations in clays [28–30]. So, apart from NTA being involved in esterification reaction with the freely available hydroxyl groups on CNCs dispersed in the layers of VCL and also with the hydroxyl group on the surface of VCL, NTA is also capable of complexing the exchangeable cations present in VCL to form VCM.

The BET surface area of VCL was 4 $m^2\ g^{-1}$ as previously reported [17] but after the modification, the surface area increased to 96 $m^2\ g^{-1}$ in VCM as shown in Fig. 5a. The tremendous increase in surface area may be accounted for as being due to the delamination of structure and development of porosity in VCM that may have resulted in change of crystalline structure creating micropores and mesopores [31, 32]. The TGA curve of VCL, CNCs and VCM is presented in Fig. 5b. The first loss in mass was noticed at temperature below 100 °C in VCL, CNCs and VCM, which was attributed to loss of water molecules physisorbed on the surface of these materials. The second loss in mass was in the range 100–200 °C that may be due to loss of internally bonded water molecules in CNCs and loss of more free water molecules in the particle spaces of VCL and VCM. Loss observed in the range 205–340 °C in CNCs may be attributed to degradation leading to 1,4 and 1,6 anhydroglucopyranoside and depolymerization at

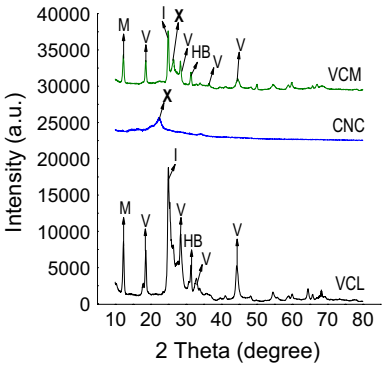

Fig. 4 XRD pattern of VCL, CNC and VCM (V: vermiculite, M: mica, I: illite, HB: hydrobiotite, **X**: CNC)

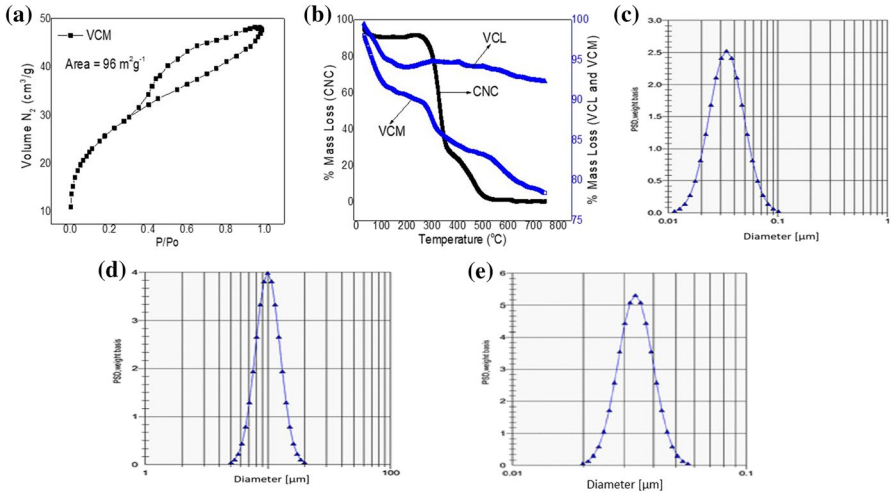

Fig. 5 **a** BET of VCM, **b** TG curves of VCL, CNC and VCM, **c** PSD of VCL, **d** PSD of VCM, **e** PSD of CNC

1,4 glycosidic bond [32]. Similar mass loss was only found in VCM at range 225–350 °C. Loss in mass at 450–800 °C in VCL may be attributed to dehydroxylation [33] while in the case of VCM it may be accounted for as being due to dehydroxylation as well as loss of char emanating from the modification with CNCs and NTA.

The particle size distribution is monomodal for the entire sample with mean size of 0.0359 µm in VCL, which increased to 10.1600 µm in VCM after the modification as shown in Fig. 5c–e. The zeta potential and SEM images are presented in Fig. 6. The zeta potential increased as the pH value increased in both VCL and VCM. These values help in quantifying the charges, degree of stability and possible electrostatic interaction at these surfaces of VCL and VCM [34, 35]. This distribution showed that VCL and VCM are stable in liquid medium with respect to solid–liquid interactions. The result presents a high zeta potential for the samples over the studied pH range. The high values correspond with previously reported high layer charges characterization for vermiculites [27], although this value reduced after the modification which may be due to the functionalization with NTA which may have complexed some of the cations at the surface of VCL. The SEM revealed both VCL and VCM to have flaky look with irregular shapes. These flakes produced some amounts of porosity in VCL before the introduction of CNCs and NTA. The dispersion of CNCs on the surface and internal layers of VCL was possible due to the nano-size dimension of CNCs and the hydrogen bonding between CNCs and the surface of VCL. The modification had influenced the densification and porosity in that few pores are on VCL as seen in the micrograph whereas more of the pores are in VCM.

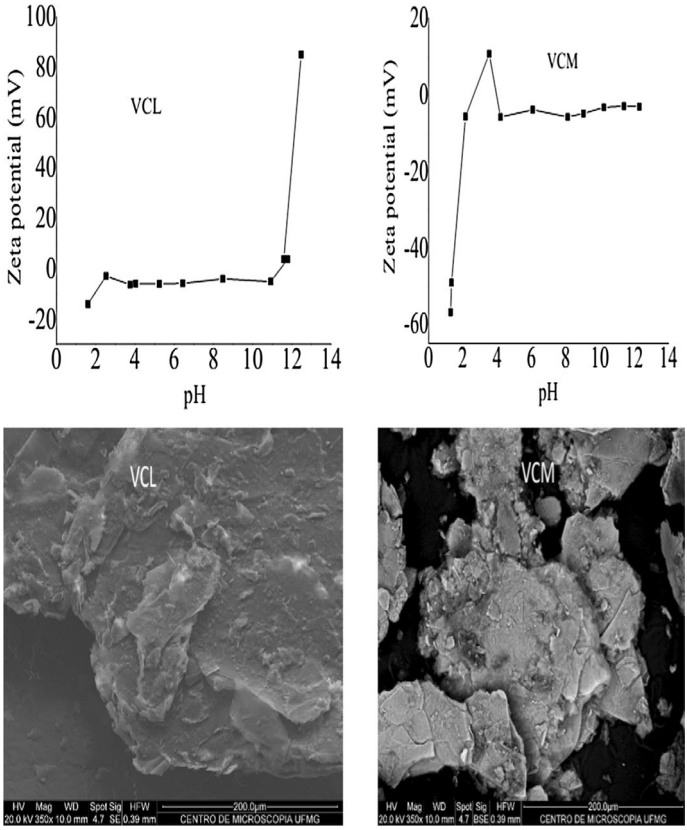

Fig. 6 Zeta potential and SEM images of VCL and VCM

Adsorption process

Effect of contact time and concentrations

The effect of contact time and concentration on the ability of VCL and VCM to remove 4-aminoantipyrine from solution is presented in Fig. 7. The removal of 4-aminoantipyrine took place gradually as equilibrium was attained at 120 min for all concentrations above 1 mg/L. It was observed that as concentration reduced, the time taken to attain equilibrium also reduced. The relatively short time of attaining equilibrium (at 120 min) suggests that the sorption of 4-aminoantipyrine on both VCL and VCM may likely be via kinetics [36, 37]. For both VCL and VCM, the percentage removal of 4-aminoantipyrine increased as concentration reduced. However, the ability of VCL to remove 4-aminoantipyrine from solution was found lower than that of VCM. The capacity to remove 4-aminoantipyrine from solution improved significantly after the modification of VCL. This was observed in the increase in the percentage removal at concentrations higher than 1 mg/L in VCM.

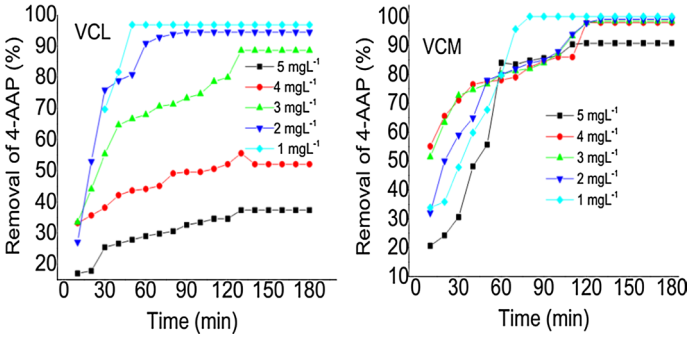

Fig. 7 Percentage removal of 4-AAP by VCL and VCM at varying concentrations. Note: 4-AAP = 4-aminoantipyrine

Vermiculites have high layer charge, which inhibits ion exchange. However, previous study has shown that acid treatment is capable of leaching the octahedral layers of vermiculites by way of protonating the oxygen atoms [38]. The treatment of VCL with NTA may have protonated the oxygen atoms in VCL, which may have resulted in increase in heterogeneity of OH species in the structure of VCM, and decreases layer charge, which may have promoted ion exchange. This change in structure must have enhanced the removal capacity of VCM toward 4-aminoantipyrine.

Adsorption kinetics

The adsorption kinetics of 4-aminoantipyrine on VCL and VCM was studied by fitting the experimental data with pseudo-first-order, pseudo-second-order, Elovich and intra-particle diffusion models. The linearized form of pseudo-first-order rate equation is [39]:

$$\mathrm{In}\left(q_e - q_t\right) = \mathrm{In}q_e - k_1 t \tag{3}$$

where q_e and q_t are concentrations of 4-aminoantipyrine at equilibrium and time t, respectively, while k_1 is the pseudo-first-order rate constant (min^{-1}). The equilibrium adsorption capacity (q_e) and k_1 were calculated from the intercept and slope of the plot of In ($q_e - q_t$) versus t.

The linearized form of the pseudo-second-order equation is [40]:

$$\frac{t}{q_t} = \frac{1}{k_2 q_e^2} + \frac{t}{q_e} \tag{4}$$

where k_2 is the adsorption rate constant (g mg^{-1} min^{-1}). The initial sorption rate was calculated as $k_2 q_e$ (mg g^{-1} min^{-1}). Equilibrium adsorption capacity (q_e) and the pseudo-second-order rate constant, k_2, were obtained from the slope and intercept of the plot of t/q_t versus t. The linearized form of Elovich equation was also used which is given as [41]:

$$q_t = \frac{1}{\beta}\mathrm{In}(\propto \beta) + \frac{1}{\beta}\mathrm{In}t \tag{5}$$

There Elovich constants α (mg g^{-1} min^{-1}) and β were calculated from the plot of q_t versus In t. Data obtained were further fitted for the Intra-particle diffusion. This was determined as described by Weber and Morris [42]:

$$q_t = k_i t^{0.5} \tag{6}$$

The rate constant, k_i (mg g^{-1} $min^{-0.5}$), was determined from the slop of the plot of q_t versus $t^{0.5}$.

The results for the different models described are shown in Table 1. The data fitted best for pseudo-second-order model, having better regression coefficients than other models considered. This suggests that the sorption of 4-aminoantipyrine on VCL and VCM follows pseudo-second-order kinetic model which indicates that the sorption process is chemically rate controlled suggesting chemisorption [43]. The adsorption capacity (q_e) obtained for the pseudo-second-order kinetic model (2.7042 mg g^{-1} for VCL and 6.5317 mg g^{-1} for VCM) compared relatively well with values obtained from the experimental results for both VCL (2.9045 mg g^{-1}) and VCM (6.5378 mg g^{-1}). This adsorption capacity values are lower that values reported for modified organo-vermiculite for the removal of *p*-nitrophenol [44] and diatomite for the removal of quinmerac [45]. However, the percentage removal exhibited by VCL and VCM reveals them as substantial materials for the treatment of water system contaminated with low amount of 4-aminoantipyrine and possibly other organic micro-pollutant at low concentrations.

The plot of q_t versus ln t for the Elovich model gave a straight line from which β was calculated to be 2.0756 mg g^{-1} for VCL and 1.7879 mg g^{-1} for VCM. The r^2 values were 0.9607 for VCL and 0.9195 for VCM which further supports the suggestion that the sorption of 4-aminoantipyrine on VCL and VCM may be via chemisorption [46].

Intra-particle diffusion further gave insight into the sorption of 4-aminoantipyrine on VCL and VCM. There is the possibility of the overall sorption process being

Table 1 Kinetic model parameters for the sorption of 4-aminoantipyrine on VCL and VCM

Model	Parameter	VCL	VCM
Pseudo-first-order	q_e (mg g^{-1})	1.7057	10.2103
	k_1 (min^{-1})	0.0162	0.0134
	r^2	0.9332	0.8336
Pseudo-second-order	q_e (mg g^{-1})	2.7042	6.5317
	k_2 (g mg^{-1} min^{-1})	0.0254	0.0032
	r^2	0.9882	0.9793
	h (mg g^{-1} min)	0.1854	0.1365
Elovich	β (g mg^{-1})	2.0756	1.7879
	α (mg g^{-1} min^{-1})	2.1231	2.4925
	r^2	0.9607	0.9195
Intra-particle diffusion	k_i (mg g^{-1} $min^{1/2}$)	0.1541	0.1710
	C (mg g^{-1})	1.4847	1.8147
	r^2	0.9791	0.9173
Experiment	q_e (mg g^{-1})	2.9045	6.5378

controlled either by one or more steps. The possibility of intra-particle diffusion was examined using the intra-particle model. The plot of q_t versus $t^{0.5}$ gave a linear plot, which suggested the presence of intra-particle diffusion during the sorption process. However, the linear plot did not pass through the origin, which indicates that intra-particle diffusion was not the sole rate-controlling step [47].

Effect of pH

The pH plays a vital role in understanding the mechanism of sorption as this affects the charges at the surface of adsorbent as well as the nature of the adsorbate in solution. As shown in Fig. 8, the adsorption capacity of VCL and VCM increased with increase in pH. Similar observation was also recorded for the percentage adsorbed. This observed sorption pattern can be accounted for as being due to the surface charge of the adsorbents (VCL and VCM) and the adsorbate (4-aminoantipyrine) at the different pH range. The isoelectric point of vermiculite has been reported as 2.57 [23]. The surface of the adsorbents may be described as follows:

$$-\mathrm{DOH} + \mathrm{H}^+ \rightleftarrows -\mathrm{DOH}_2^+ \,[\text{Protonation}] \tag{7}$$

$$-\mathrm{DOH} + \mathrm{OH}^- \rightleftarrows -\mathrm{DO}^- + \mathrm{H_2O}\,\left[\text{Deprotonation}\right] \tag{8}$$

$$-\mathrm{DO}^- = -\mathrm{DOH}_2^+\,\left[\text{Isoelectric point}\right] \tag{9}$$

where –D represents the surface of the adsorbents. In acidic medium (low pH), the surface can be described to be protonated as shown in Eq. 7. When in basic medium (high pH), the surface can be considered to be deprotonated as shown in Eq. 8 while the isoelectric point is represented in Eq. 9. The surfaces of the adsorbents were negatively charged at high pH which promoted the interaction with 4-aminoantipyrine which was positively charged at high pH. As seen in Fig. 8, the sorption of 4-aminoantipyrine by both adsorbents increased with increase in pH. Therefore, with increase in pH value, there was increase in the amount of 4-aminoantipyrine adsorbed by the adsorbents as a result of the increase in the electrostatic interaction between the surfaces of the adsorbents and 4-aminoantipyrine. However, the higher adsorption capacity exhibited by VCM over VCL may be due to the additional

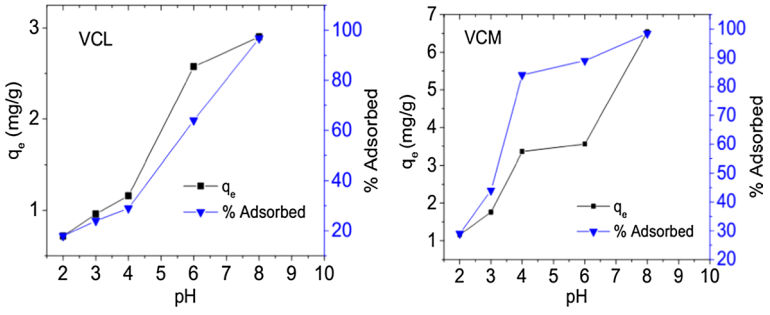

Fig. 8 Effect of pH on the removal of 4-aminoantipyrine by VCL and VCM

contribution from –COOH species on its surface resulting from the treatment with NTA. This additional contribution at higher pH may be described as:

$$-\mathrm{DCOOH} + \mathrm{OH}^- \rightleftarrows -\mathrm{DCOO}^- + \mathrm{H_2O}\ [\mathrm{Deprotonation}] \tag{10}$$

This increases the negative charges at the surface of VCM, which further enhances its ability to remove 4-aminoantipyrine from solution. Moreover, treatment with NTA may have caused leaching of layer components and loss of CEC may be compensated by the observed increase in surface area and formation of adsorption centers or pores [27]; these adsorption centers may have also played a role in trapping some amount of 4-aminoantipyrine.

Adsorption isotherms

The experimental data were fitted with Langmuir, Freundlich and Temkin isotherm models. The Langmuir isotherm explains the existence of maximum limitation uptake, which reflects a saturated monolayer of 4-aminoantipyrine species at the surface of VCL and VCM with an assumption of uniform energies of adsorption. The linear representation of the Langmuir isotherm model is expressed as:

$$\frac{C_\mathrm{e}}{q_\mathrm{e}} = \frac{1}{Q_\mathrm{o}} C_\mathrm{e} + \frac{1}{K_\mathrm{L}} Q_\mathrm{o} \tag{11}$$

C_e (mg/L) represents the equilibrium concentration of 4-aminoantipyrine, Q_o (mg g^{-1}) is the maximum monolayer coverage capacity, q_e (mg g^{-1}) is the amount of 4-aminoantipyrine adsorbed at equilibrium and K_L (L mg^{-1}) is the Langmuir isotherm constant. A linear plot was obtained when $C_\mathrm{e}/q_\mathrm{e}$ was plotted against C_e with a slope of $1/Q_\mathrm{o}$ and an intercept of $1/Q_\mathrm{o}K_\mathrm{L}$. The essential features of the Langmuir isotherm (R_L) may be expressed as:

$$R_\mathrm{L} = \frac{1}{1 + \left(1 + K_\mathrm{L} C_\mathrm{o}\right)} \tag{12}$$

where C_o is the initial concentration and K_L is the constant related to the energy of adsorption (Langmuir constant). When $R_\mathrm{L} > 1$ adsorption nature is considered to be unfavorable, linear if $R_\mathrm{L} = 1$, favorable if $0 < R_\mathrm{L} < 1$ and irreversible if $R_\mathrm{L} = 0$. R_L was 0.0041 for VCL and 0.0446 for VCM indicating a favorable process, which was monolayer. As shown in Table 2, the higher value of K_L in VCL than that of VCM shows a higher heat of sorption and stronger bond of sorption of 4-aminoantipyrine at the surface of VCL. This also means that VCL holds 4-aminoantipyrine stronger at its surface than VCM does.

Freundlich isotherm describes an empirical relationship between the concentrations of 4-aminoantipyrine at the surfaces of VCL and VCM. This can be expressed as:

$$q_\mathrm{e} = K_\mathrm{f} C_\mathrm{e}^n \tag{13}$$

The model assumes that adsorption occurs on heterogeneous surface via multilayer sorption mechanism and the amount of 4-aminoantipyrine adsorbed increase

Table 2 4-Aminoantipyrine sorption parameters for Langmuir, Freundlich and Temkin models

Isotherm	Parameter	
	VCL	VCM
Langmuir		
Q_o (mg g^{-1})	3.3344	6.5359
K_L (L mg^{-1})	59.980	5.1000
r^2	1.0000	1.0000
R_L	0.0041	0.0446
Freundlich		
K_f	7.1846	2.9147
$1/n$	1.2659	0.3026
r^2	0.9824	0.9785
Temkin		
A (L g^{-1})	5.2894	2.9113
B	3.3128	1.2675
R^2	0.9964	0.9869

with concentration. Where q_e (mg g^{-1}) is the amount of 4-aminoantipyrine adsorbed at equilibrium, K_f (mg g^{-1}) is the Freundlich isotherm constant, C_e (mg L^{-1}) is the equilibrium concentration of 4-aminoantipyrine and n is the adsorption intensity. The values obtained for the Freundlich parameters are presented in Table 2. Considering the Freundlich model, adsorption capacity can be explained as a function of $1/n$. Previous work has shown that when $1/n = < 1$, the process can be said to be a normal adsorption, if $1/n = 1$ then the partition between the liquid and solid phases are independent of concentration and if $1/n = > 1$ the process can be considered to be a cooperative adsorption [48]. 1/n was found to be 1.2659 for VCL and 0.3026 for VCM, respectively; which suggests a cooperative and normal adsorption, respectively.

Temkin isotherm model suggests adsorbent–adsorbate interaction and a linear decrease in heat of sorption with surface coverage [49] which is given as:

$$q_e = \left(\frac{RT}{b}\right)\mathrm{In}\left(AC_e\right) \tag{14}$$

$$q_e = B\mathrm{In}A + B\mathrm{In}C_e \tag{15}$$

where b is the Temkin isotherm constant, A (L g^{-1}) represents Temkin isotherm equilibrium binding constant and constant B (J mol^{-1}) $= RT/b$ is the constant related to heat of sorption. T is the absolute temperature (K) and R stands for gas constant (8.314 J mol^{-1} K^{-1}). Plot of q_e against ln C_e gave a straight line from which B and A were determined from slope and intercept. Values obtained are shown in Table 2. The isotherm equilibrium binding constant and constant related to heat of sorption were found higher in VCL than VCM which further corroborated the preference 4-aminoantipyrine had for VCL over VCM. The correlation coefficients (r^2) obtained for the three tested models conformed to experimented data with Langmuir

model fitting best with r^2 value 1.0000. This suggests a monolayer adsorption process.

Thermodynamics of adsorption

Thermodynamic parameters for the sorption of 4-aminoantipyrine by VCL and VCM were examined and are presented in Table 3. Parameters determined included Gibb's free energy change (ΔG^{o}), entropy change (ΔS^{o}) and enthalpy change (ΔH^{o}). The adsorption equilibrium constant (b_o) was estimated from the expression:

$$b_o = \frac{q_e}{C_e} \tag{16}$$

$$\Delta G^{o} = -RT\ln b_o \tag{17}$$

$$\Delta G^{o} = \Delta H^{o} - T\Delta S^{o} \tag{18}$$

R is the universal gas constant (8.314 J mol^{-1} K^{-1}), q_e is the adsorption capacity of VCL or VCM at equilibrium, C_e is the equilibrium concentration of 4-aminoantipyrine and T is the absolute temperature in Kelvin. ΔH^{o} and ΔS^{o} were obtained from the slope and intercept of the plot of ln b_o against reciprocal of temperature ($1/T$). The percentage removal of 4-aminoantipyrine by VCL and VCM decreased as temperature increased. The values of q_e obtained for VCL and VCM reduced as temperature increased while the values for the Gibb's free energy increased with increase in temperature. The negative nature of ΔG^{o} is an indication that the sorption of 4-aminoantipyrine by VCL and VCM is a spontaneous reaction. Results obtained for ΔH^{o} and ΔS^{o} are shown in Table 4. Both ΔH^{o} and ΔS^{o} are negative for VCL (ΔH^{o} was -57.177 kJ mol^{-1} and was ΔS^{o} -0.179 kJ mol^{-1}) and VCM (ΔH^{o} was -29.701 kJ mol^{-1} and was ΔS^{o} -0.089 kJ mol^{-1}). These negative values are an indication that the sorption process is spontaneous at low temperature but non-spontaneous at high temperature. The negative nature of ΔH^{o} further suggests the

Table 3 ΔG, percentage removal and q_e obtained at various temperatures for VCL and VCM

VCL					
T (K)	298	303	313	318	323
q_e (mg g^{-1})	2.905	2.340	2.900	1.400	1.040
Removal (%)	96.820	78.000	74.000	35.000	26.000
ΔG (kJ mol^{-1} K^{-1})	−3.746	−2.849	−1.056	−0.160	0.737
VCM					
T (K)	298	303	313	318	323
q_e (mg g^{-1})	6.538	3.676	2.840	2.900	2.500
Removal (%)	98.410	91.900	71.000	72.000	63.000
ΔG (kJ mol^{-1} K^{-1})	−3.298	−2.855	−1.969	−1.526	−1.083

Table 4 Thermodynamic parameters obtained from plot of ln b_o versus $1/T$ for VCL and VCM

Parameters	VCL	VCM
ΔH (kJ mol^{-1})	−57.177	−29.701
ΔS (kJ mol^{-1} K^{-1})	−0.179	−0.089

process to be exothermic while the negative values for ΔS^o is an indication of a stable configuration of 4-aminoantipyrine on the surfaces of VCL and VCM.

Desorption

The desorption process evaluated the removal of 4-aminoantipyrine from the surface of VCL and VCM with the aim of reuse. This involves understanding the regeneration capacity of VCL and VCM. This was achieved using ethanol, distilled water, benzene, 0.5 M HCl, 0.5 M NaOH and acetone as solvents for removing 4-aminoantipyrine from the surface of VCL and VCM. The results obtained for desorption of 4-aminoantipyrine from VCL and VCM are presented in Fig. 9. 4-Aminoantipyrine was best desorbed from VCL (60%) and VCM (76%) using water. Regeneration capacity was found lower when benzene and acetone were used as solvent for VCL, whereas the least desorption capacity was obtained using acetone. Distilled water may be considered as a potential solvent for the solvent regeneration of VCL and VCM loaded with 4-aminoantipyrine.

Quantum chemical computations

Quantum chemical computational analysis helped in understanding and describing the adsorption of 4-aminoantipyrine on VCL and VCM in molecular terms. DFT may be applied in discussing the electronic structural changes that occurs during adsorption process. Presently, DFT was applied to describe a theoretical framework in identifying the contributions of 4-aminoantipyrine adsorption mechanisms

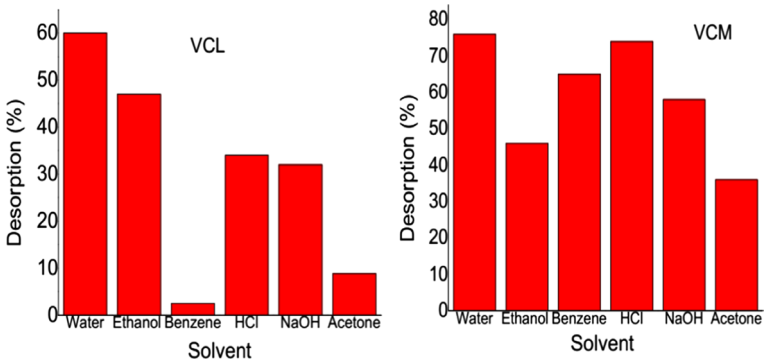

Fig. 9 Desorption of 4-aminoantipyrine from VCL and VCM

and strength. The DFT was performed at B3LYP/6-31G level theory using Spartan 14.1 software. The geometry optimization was followed by modeling the molecular electronic structures and the distribution of frontier molecular orbitals in order to establish the reactivity of 4-aminoantipyrine as well as its active sites. Figure 10 presents the optimized geometry, HOMO density distribution, LUMO density distribution, Mulliken charge population analysis, total electron distribution, electrostatic potential map, local ionization potential map as well as the LUMO map of 4-aminoantipyrine.

The LUMO and HOMO are distributed over the molecule of 4-aminoantipyrine due to the presence of lone pairs of electron from nitrogen, and oxygen and the π-electrons in its molecule. Region of highest electron density (HOMO) is possible site at which electrophiles attack, such sites are the active or adsorption centers with the utmost energy to bond to the surface of VCL and VCM. However, the LUMO orbital of 4-aminoantipyrine accepts electrons from the orbital of the constituent transition elements (Ti and Fe) in VCL and VCM using antibonding orbitals

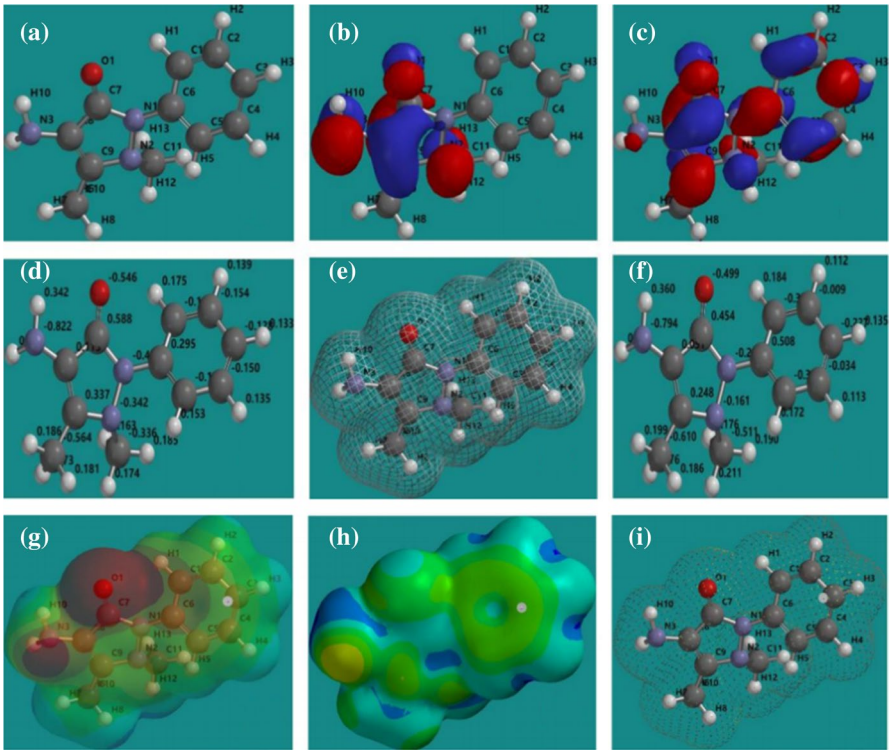

Fig. 10 Electronic properties of 4-aminoantipyrine. **a** Optimized structure of 4-aminoantipyrine, **b** HOMO density distribution of 4-aminoantipyrine, **c** LUMO density distribution of 4-aminoantipyrine, **d** Mulliken charge population analysis of 4-aminoantipyrine, **e** Total electron density of 4-aminoantipyrine, **f** Electrostatic charge of 4-aminoantipyrine, **g** Electrostatic potential map of 4-aminoantipyrine, **h** Local ionization potential map of 4-aminoantipyrine, **i** LUMO map of 4-aminoantipyrine. Note: C = carbon, H = hydrogen, O = oxygen and N = nitrogen

to form feedback bonds [50]. The presence of these adsorption centers are capable of forming flat orientation of 4-aminoantipyrine molecules on the surfaces of VCL and VCM, which may have given rise to the surface coverage by the molecule of 4-aminoantipyrine. The nitrogen and oxygen atoms present in 4-aminoantipyrine are most probably the reactive site for its sorption on the surfaces of VCL and VCM. This further suggests the interaction between the surfaces of VCL/VCM and 4-aminoantipyrine to occur via donor–acceptor interactions among lone pairs of electron, π-electrons and the vacant *d*-orbital of the constituent transition metal in VCL/VCM. The higher adsorption capacity observed in VCM must have been due to addition interaction between the heteroatoms in 4-aminoantipyrine and the carboxyl functional groups on VCM. The computed Mulliken atomic charges are as presented in Table 5. As seen in Fig. 10, nitrogen, oxygen and a few carbon atoms are negatively charged. The more negatively charged the atoms of the adsorbed center, the more readily they are available to interact with surfaces of VCL/VCM and the easily such atoms donate their electrons to unoccupied orbitals in constituent transition metal in VCL/VCM [51]. The Mulliken atomic charges revealed that molecule of 4-aminoantipyrine possess atoms that are capable of donating electrons to the orbital of constituent transition metals of VCL/VCM for bonding. These electrons are also available for covalent bonding with functional groups at the surfaces of VCL and VCM.

Reactivity of 4-aminoantipyrine may be related to frontier molecular orbitals. The higher HOMO energy of 4-aminoantipyrine may mean higher electron donating capacity to low energy empty molecular orbital of transition metals in VCL/VCM. On the other hand, LUMO energy is related to susceptibility of 4-aminoantipyrine molecule to nucleophilic attack and electron affinity. So electron-accepting capacity becomes stronger with lower LUMO energy. The energy gap (ΔE) was calculated as:

$$\Delta E = E_{\mathrm{LUMO}} - E_{\mathrm{HOMO}} \tag{19}$$

The value of the energy gap is an indication of electronic interaction. The lower the value, the better the interaction and hence sorption of 4-aminoantipyrine from solution. The value obtained for 4-aminoantipyrine is 4.32 eV. This value is within the range previously reported for the sorption of plant extract on metal surface [52];

Table 5 Molecular properties of 4-aminoantipyrine calculated using DFT at B3LYP/6-31G basis set level

Quantum chemical property	Value
Molecular surface area (Å^2)	233.81
Energy (au)	− 665.996
E_{HOMO} (eV)	− 5.12
E_{LUMO} (eV)	− 0.80
$E_{\mathrm{LUMO-HOMO}}$ (eV)	4.32
Dipole moment (debye)	6.55
Volume (Å^3)	213.65
Polarizability	57.68
η (eV)	2.16

the value is higher than what was reported for methionine and phenylalanine [53] but lower than what was reported for *Piper guineense* extract [54]. Dipole moment also describes sorption process; when it is high, it is an indication that adsorption process is favored. The dipole moment for 4-aminoantipyrine was found to be 6.55 debye. Absolute hardness (η) is important in measuring the reactivity and stability of 4-aminoantipyrine. It was calculated as:

$$\eta = \frac{E_{\mathrm{LUMO}} - E_{\mathrm{HOMO}}}{2} \tag{20}$$

Adsorption of 4-aminoantipyrine took place on surface of VCL/VCM at regions on 4-aminoantipyrine molecule with greatest softness and lowest hardness. Hard molecules have large energy gap while soft molecules does not. This makes soft molecules more reactive than hard molecules [55].

Conclusion

The wastewater purifying capacity of VCL was enhanced by way of chemical modification using CNCs and NTA via simple reaction to produce VCM. Both VCL and VCM were characterized and investigated as adsorbent for the removal of 4-aminoantipyrine from aqueous solution. After the modification, the BET surface area of VCL increased from 4 to 96 $m^2\ g^{-1}$ in VCM. The adsorption capacity of VCM (6.5378 mg g^{-1}) was found higher than that of VCL (2.9045 mg g^{-1}). The sorption process of VCL and VCM was chemisorptive, monolayer and spontaneous. Quantum chemical computational analysis was also used to understand and describe the sorption of 4-aminoantipyrine on VCL and VCM in molecular terms. It was found that the LUMO and HOMO are distributed over the molecule of 4-aminoantipyrine due to the presence of lone pairs of electron from nitrogen, and oxygen and the π-electrons in its molecule which aid its sorption on VCL and VCM. This interaction between the surfaces of VCL/VCM and 4-aminoantipyrine occurred via donor–acceptor interactions among lone pairs of electron, π-electrons and the vacant *d*-orbital of the constituent transition metal in VCL/VCM. The results suggest VCM as a potential resource for the removal of pharmaceutical pollutants from water system.

Acknowledgements Author will like to thank TWAS-CNPq for the provision of postdoctoral fellowship. Author is also grateful for the support received from Prof. Pereira Vargas Fabiano and the Department of Chemistry, Universidade Federal de Minas Gerais, Minas Gerais, Brazil.

References

1. Putra EK, Pranowo R, Sunarso J, Indraswati N, Ismadji S (2009) Performance of activated carbon and bentonite for adsorption of amoxicillin from wastewater: mechanisms, isotherms and kinetics. Water Res 43:2419–2430. https://doi.org/10.1016/j.watres.2009.02.039
2. Kawahara Y (1993) Immobilization of glucose oxidase in wild silk fiber (*Antheraea pernyi*) treated with an alkaline solution. J Seric Sci Jpan 62:272–275

3. Wang F, Zhang Y-Q (2015) Chapter eight—bioconjugation of silk fibroin nanoparticles with enzyme and peptide and their characterization. Adv Protein Chem Struct Biol 98:263–291. https://doi.org/10.1016/bs.apcsb.2014.11.005
4. Deshmukh P, Soni PK, Kankoriya A, Halve AK, Dixit R (2015) 4-Aminoantipyrine: a significant tool for the synthesis of biologically active schiff bases and metal complexes. Int J Pharm Sci Rev Res 34:162–170
5. Alam MS, Lee DU (2016) Physicochemical analyses of a bioactive 4-aminoantipyrine analogue—synthesis, crystal structure, solid state interactions, antibacterial, conformational and docking studies. EXCLI J 15:614–629. https://doi.org/10.17179/excli2016-477
6. Hamdaoui O, Naffrechoux E (2007) Modeling of adsorption isotherms of phenol and chlorophenols onto granular activated carbon Part I. Two-parameter models and equations allowing determination of thermodynamic parameters. J Hazard Mater 147:381–394. https://doi.org/10.1016/j.jhazmat.2007.01.021
7. Ismadji S, Soetaredjo FE, Ayucitra A (2015) Clay materials for environmental remediation. Springer, Berlin
8. Lagaly G (1982) Layer charge heterogeneity in vermiculites. Clays Clay Miner 30:215–222
9. Guggenheim S, Adams JM, Bain DC, Bergaya F, Bigatti MF, Drits VA, Formoso MLL, Galán E, Kogue T, Stanjek H (2006) Summary of recommendations of nomenclature committees relevant to clay mineralogy: report of the association internationale pour L'Étude des Argiles (AIPEA) nomenclature committee for 2006. Clays Clay Miner 54:761–772; Clay Miner 41:863–877
10. Valášková M, Martynková GS (2012) Vermiculite: structural properties and examples of the use. In: Valaskova Marta (ed) Clay minerals in nature: their characterization, modification and application. InTech, Rijeka, pp 210–238. https://doi.org/10.5772/51237
11. Weiss Z, Valvoda V, Chmielová M (1994) Dehydration and rehydration of natural mgvermiculite. Geol Carpath 45:33–39
12. de la Calle C, Suquet H, Pons CH (1988) Stacking order in 14.30 Å Mg-vermiculite. Clays Clay Miner 36:481–490
13. Medeiros MA, Sansiviero MTC, Araujo MH, Lago RM (2009) Modification of vermiculite by polymerization and carbonization of glycerol to produce highly efficient materials for oil removal. Appl Clay Sci 45:213–219. https://doi.org/10.1016/j.clay.2009.06.008
14. Moura FCC, Lago RM (2009) Catalytic growth of carbon nanotubes and nanofibers on vermiculite to produce floatable hydrophobic 'nanosponges' for oil spill remediation. Appl Catal B Environ 90:436–440. https://doi.org/10.1016/j.apcatb.2009.04.003
15. Zhang H, Yu J, Kuang D (2012) Effect of expanded vermiculite on aging properties of bitumen. Constr Build Mater 26:244–248. https://doi.org/10.1016/j.conbuildmat.2011.06.017
16. de Mesquita JP, Reis LS, Purceno AD, Donnici CL, Lago RM, Pereira FV (2013) Carbon-clay composite obtained from the decomposition of cellulose nanocrystals on the surface of expanded vermiculite. J Chem Technol Biotechnol 88:1130–1135. https://doi.org/10.1002/jctb.3952
17. Wang J, Gao M, Ding F, Shen T (2018) Organo-vermiculites modified by heating and gemini pyridinium surfactants: preparation, characterization and sulfamethoxazole adsorption. Colloids Surf A Physicochem Eng Asp 546:143–152. https://doi.org/10.1016/j.colsurfa.2018.03.014
18. Wu C-N, Saito T, Fujisawa S, Fukuzumi H, Isogai A (2012) Ultrastrong and high gas-barrier nanocellulose/clay-layered composites. Biomacromol 13:1927–1932. https://doi.org/10.1021/bm300465d
19. de Mesquita JP, Donnici CL, Pereira FV (2010) Biobased nanocomposites from layer-by-layer assembly of cellulose nanowhiskers with chitosan. Biomacromol 11:473–480. https://doi.org/10.1021/bm9011985
20. El Mouzdahir Y, Elmchaouri A, Mahbouba R, Gilb A, Korili SA (2009) Synthesis of nano-layered vermiculite of low density by thermal treatment. Powder Technol 189:2–5. https://doi.org/10.1016/j.powtec.2008.06.013
21. Sutcu M (2015) Influence of expanded vermiculite on physical properties and thermal conductivity of clay bricks. Ceram Inter 41:2819–2827. https://doi.org/10.1016/j.ceramint.2014.10.102
22. Duman O, Tunç S, Polat TG (2015) Determination of adsorptive properties of expanded vermiculite for the removal of C. I. Basic Red 9 from aqueous solution: kinetic, isotherm and thermodynamic studies. Appl Clay Sci 109–110:22–32. https://doi.org/10.1016/j.clay.2015.03.003
23. Duman O, Tunç S (2008) Electrokinetic properties of vermiculite and expanded vermiculite: effects of pH, clay concentration and mono- and multivalent electrolytes. Sep Sci Technol 43:3755–3776. https://doi.org/10.1080/01496390802219109

24. Adewuyi A, Pereira FV (2017) Chemical modification of cellulose isolated from underutilized *Hibiscus sabdariffa* via surface grafting: a potential bio-based resource for industrial application. Kemija u industriji 66:327–338. https://doi.org/10.15255/KUI.2016.024
25. Muiambo HF, Focke WW, Atanasova M, Westhuizen IV, Tiedt LR (2010) Thermal properties of sodium-exchanged palabora vermiculite. Appl Clay Sci 50:51–57. https://doi.org/10.1016/j.clay.2010.06.023
26. Macheca AD, Focke WW, Muiambo HF, Kaci M (2016) Stiffening mechanisms in vermiculite–amorphous polyamide bio-nanocomposites. Eur Polym J 74:51–63. https://doi.org/10.1016/j.eurpolymj.2015.11.013
27. Stawinski W, Freitas O, Chmielarz L, Wegrzyn A, Komedera K, Błachowski A, Figueiredo S (2016) The influence of acid treatments over vermiculite based material as adsorbent for cationic textile dyestuffs. Chemosphere 153:115–129. https://doi.org/10.1016/j.chemosphere.2016.03.004
28. Muir IJ, Nesbitt HW (1991) Effects of aqueous cations on the dissolution of labradorite feldspar. Geochim Cosmochim Acta 55:3181–3189. https://doi.org/10.1016/0016-7037(91)90482-K
29. Huang W-L, Longo JM (1992) The effect of organics on feldspar dissolution and the development of secondary porosity. Chem Geol 98:271–292. https://doi.org/10.1016/0009-2541(92)90189-C
30. Fein JB (1994) Porosity enhancement during clastic diagenesis as a result of aqueous metal-carboxylate complexation: experimental studies. Chem Geol 115:263–279. https://doi.org/10.1016/0009-2541(94)00003-Q
31. Santos SSG, Silva HRM, de Souza AG, Alves APM, da Silva Filho EC, Fonseca MG (2015) Acid-leached mixed vermiculites obtained by treatment with nitric acid. Appl Clay Sci 104:286–294. https://doi.org/10.1016/j.clay.2014.12.008
32. Sharma RK (2012) A study in thermal properties of graft copolymers of cellulose and methacrylates. Adv Appl Sci Res 3:3961–3969
33. Balima F, Nguyen A-N, Reinert L, Floch SL, Pischedda V, Duclaux L, San-Miguel A (2015) Effect of the temperature on the structural and textural properties of a compressed K-vermiculite. Chem Eng Sci 134:555–562. https://doi.org/10.1016/j.ces.2015.05.061
34. Salopek B, Krasic D, Filipovic S (1992) Measurement and application of zeta-potential. Rudarsko-geolosko-naftni zbornik 4:147–151. https://hrcak.srce.hr/24757
35. Hanaor DAH, Michelazzi M, Leonelli C, Sorrell CC (2012) The effects of carboxylic acids on the aqueous dispersion and electrophoretic deposition of ZrO_2. J Eur Ceram Soc 32:235–244. https://doi.org/10.1016/j.jeurceramsoc.2011.08.015
36. Lazaridis NK, Karapantsios TD, Georgantas D (2003) Kinetic analysis for the removal of a reactive dye from aqueous solution onto hydrotalcite by adsorption. Water Res 37:3023–3033. https://doi.org/10.1016/S0043-1354(03)00121-0
37. Oladoja NA, Adelagun ROA, Ahmad AL, Unuabonah EI, Bello HA (2014) Preparation of magnetic, macro-reticulated cross-linked chitosan for tetracycline removal from aquatic systems. Colloids Surf B Biointerfaces 117:51–59. https://doi.org/10.1016/j.colsurfb.2014.02.006
38. Schoonheydt RA, Johnston CT (2006) Surface and interface chemistry of clay minerals. In: Bergaya F, Theng BKG, Lagal G (eds) Handbook of clay science. Elsevier, Amsterdam
39. Lagergren S (1898) About the theory of so-called adsorption of soluble substances. Kungliga Svenska Vetenskapsakademiens Handlingar 24:1–39
40. Alhamed YA (2009) Adsorption kinetics and performance of packed bed adsorber for phenol removal using activated carbon from dates' stones. J Hazard Mater 170:763–770. https://doi.org/10.1016/j.jhazmat.2009.05.002
41. Shek TH, Ma A, Lee VKC, McKay G (2009) Kinetics of zinc ions removal from effluents using ion exchange resin. Chem Eng J 146:63–70. https://doi.org/10.1016/j.cej.2008.05.019
42. Weber WJ, Morris JC (1963) Kinetics of adsorption on carbon solution. J Sanit Eng Div Am Soc Civ Eng 89:31–59
43. Ho YS, McKay G (1999) Pseudo-second order model for sorption processes. Proc Biochem 34:451–465. https://doi.org/10.1016/S0032-9592(98)00112-5
44. Yu M, Gao M, Shen T, Wang J (2018) Organo-vermiculites modified by low-dosage Gemini surfactants with different spacers for adsorption toward p-nitrophenol. Colloids Surf A Physicochem Eng Asp 553:601–611. https://doi.org/10.1016/j.colsurfa.2018.08.001
45. Khaldi K, Hadjel M, Benyoucef A (2018) Removal of quinmerac by diatomite and modified diatomite from aqueous solution. Surf Engin Appl Electrochem 54:194–202. https://doi.org/10.3103/S1068375518020084

46. Wu F-C, Tseng R-L, Juang R-S (2009) Characteristics of Elovich equation used for the analysis of adsorption kinetics in dye-chitosan systems. Chem Eng J 150:366–373. https://doi.org/10.1016/j.cej.2009.01.014
47. Hameed BH, Mahmoud DK, Ahmad AL (2008) Equilibrium modeling and kinetic studies on the adsorption of basic dye by a low-cost adsorbent: coconut (*Cocos nucifera*) bunch waste. J Hazard Mater 158:65–72. https://doi.org/10.1016/j.jhazmat.2008.01.034
48. Mohan S, Karthikeyan J (1997) Removal of lignin and tannin color from aqueous solution by adsorption on to activated carbon solution by adsorption on to activated charcoal. Environ Pollut 97:183–187. https://doi.org/10.1016/S0269-7491(97)00025-0
49. Tempkin MI, Pyzhev V (1940) Kinetics of ammonia synthesis on promoted iron catalyst. Acta Phys Chim USSR 12:327–356
50. Obot IB, Obi-Egbedi NO, Ebenso EE, Afolabi AS, Oguzie EE (2013) Experimental, quantum chemical calculations, and molecular dynamic simulations insight into the corrosion inhibition properties of 2-(6-methylpyridin-2-yl)oxazolo [5,4-f] [1, 10]phenanthroline on mild steel. Res Chem Intermed 39:1927–1948. https://doi.org/10.1007/s11164-012-0726-3
51. Obi-Egbedi NO, Obot IB, El-Khaiary MI (2011) Quantum chemical investigation and statistical analysis of the relationship between corrosion inhibition efficiency and molecular structure of xanthene and its derivatives on mild steel in sulphuric acid. J Mol Struct 1002:86–96. https://doi.org/10.1016/j.molstruc.2011.07.003
52. Njoku DI, Ukaga I, Ikenna OB, Oguzie EE, Oguzie KL, Ibisi N (2016) Natural products for materials protection: corrosion protection of aluminium in hydrochloric acid by Kola nitida extract. J Mol Liq 219:417–424. https://doi.org/10.1016/j.molliq.2016.03.049
53. Oguzie EE, Li Y, Wang SG, Wanga F (2011) Understanding corrosion inhibition mechanisms-experimental and theoretical approach. RSC Adv 1:866–873. https://doi.org/10.1039/c1ra00148e
54. Oguzie EE, Adindu CB, Enenebeaku CK, Ogukwe CE, Chidiebere MA, Oguzie KL (2012) Natural products for materials protection: mechanism of corrosion inhibition of mild steel by acid extracts of *Piper guineense*. J Phys Chem C 116:13603–13615. https://doi.org/10.1021/jp300791s
55. Lesar A, Milosev I (2009) Density functional study of the corrosion inhibition properties of 1,2,4-triazole and its amino derivatives. Chem Phys Lett 483:198–203. https://doi.org/10.1016/j.cplett.2009.10.082